Feature Based Automated Detection of COVID-19 from Chest X-Ray Images

Chapter · January 2021

CITATION
1

READS
106

2 authors:

Shawli Bardhan
IIIT Una
14 PUBLICATIONS **65** CITATIONS
SEE PROFILE

Dr. Sukanta Roga
Visvesvaraya National Institute of Technology
28 PUBLICATIONS **165** CITATIONS
SEE PROFILE

Feature Based Automated Detection of COVID-19 from Chest X-Ray Images

Shawli Bardhan and Sukanta Roga

Abstract Nowadays the biggest challenge for health care is controlling the pandemic of Coronavirus disease 2019 (COVID-19). Radiological investigation combining with machine learning can serve as a standardized methodology for detecting COVID-19. Chest X-ray imaging is the most feasible radiological test for COVID-19. Machine learning-based automated classification of COVID-19 from chest X-ray images can act as an assistive method to the medical experts for accurate diagnosis of disease. Aiming at this, the study focused on developing a simplified method of X-ray image based computerized COVID-19 detection through conventional feature extraction and classification approach. The method of X-ray image based COVID-19 detection consists of only two main steps: feature extraction, and classification. In feature extraction, a total of 55 X-ray image texture features is extracted from seven different groups. Classification of COVID-19 has been performed using those extracted features through four different popularly used classifiers. The overall analysis of the study has been performed over two datasets. The Random Forest classifier generates the best accuracy of 98.6% and 98.9% for dataset 1 and 2 with the area under the curve (AUC) values 0.99 and 1 respectively. The outcome of our study provides optimal accuracy of COVID-19 classification using X-ray images compare to existing popular studies in this domain. The reliable and less-complex feature of the proposed method may serve it as a computerized X-ray image based COVID-19 detection mechanism, especially in rural areas where medical experts are not available.

Keywords COVID-19 · X-ray image · Feature extraction · Classification · Detection

S. Bardhan (✉)
Department of Computer Science, Indian Institute of Information Technology Una, Una, Himachal Pradesh, India
e-mail: shawli.cse@gmail.com

S. Roga
Department of Mechanical Engineering, Visvesvaraya National Institute of Technology, Nagpur, Maharashtra, India
e-mail: rogasukanta@gmail.com

I. Arpaci et al. (eds.), *Emerging Technologies During the Era of COVID-19 Pandemic*, Studies in Systems, Decision and Control 348,
https://doi.org/10.1007/978-3-030-67716-9_8

1 Introduction

The Coronavirus disease 2019 (COVID-19) comes under the communicable category and spreading all over the world with rapid growth. At the ending of 2019, the COVID-19 was first found in Wuhan city of China as pneumonia. The perilous disease syndromes in the human body are similar to Severe Acute Respiratory Syndrome (SARS). Due to COVID, patients go through syndromes like cough, fever, sore throat, fatigue, headache, shortness of breathing, muscle pain, etc. [1]. In the present scenario, COVID-19 is wide spreader around the world. According to the report of the World Health Organization (WHO), the outbreak of the disease infected a vast number of people, and death and affected cases are rapidly increasing each day. The total number of death due to COVID-19 reaches 3,49,095 and total infected cases are 54,88, 825 [2]. A total of 217 countries are under the epidemic of COVID-19. The gold standard for the diagnosis of COVID-19 is the reverse-transcription polymerase chain reaction (RT-PCR) test [3, 4]. But the sensitivity of the RT-PCR test is not satisfactory. The negative test outcome through RT-PCR does not interpret the complete absence of the COVID virus in the body [4–6]. So, medical imaging is popularly used as a complementary modality for the diagnosis of COVID-19. X-ray, computed tomography (CT), lung ultrasound, magnetic resonance imaging (MRI) [7, 8] plays a vital role in the area of COVID-19 diagnosis. Among the above-mentioned imaging techniques, CT and X-rays are most popular for COVID-19. However, CT imaging contains negative issues related to a shortage of CT facilities in a rural area, the cost of CT imaging, etc. Chest X-ray is a low-cost and available imaging methodology, and will likely be the frequently utilized imaging modality for detection and monitoring COVID-19 related abnormality. Generally image features like lung consolidation, lesions with ground-glass opacities, pulmonary fibrosis, multiple lesions, bilateral lower lobe consolidations, peripheral air space opacities, diffuse air space, etc. are indicating characteristics for COVID-19 positive [9–12]. The use of X-ray imaging for identification of the above mentioned features can act as a key diagnosis method for COVID-19 and also for monitoring the progress of treatment. A combination of artificial intelligence (AI) and imaging technology can further strengthen the capacity of X-ray image analysis for the identification of COVID-19 characteristics and also help in the computerized image-based diagnosis of the disease.

Seeing the present necessity of computerized COVID-19 detection, the study aims to classify normal and COVID-19 X-ray images by extracting textures features of images. The advantage of the study includes methodological simplicity with higher accuracy compared to existing popular researches (Table 1).

The rest of the paper is organized as Sect. 2 describes the existing image analysis-oriented research on COVID-19. Section 3 details the methodology of the study. Sections 4 and 5 contains the result and discussion respectively. Finally, Sect. 6 concludes the overall study directing the future scope.

Table 1 Literature review on X-ray image analysis based COVID-19 classification

Literature	Aim	Method	Subjects	Accuracy (%)/Result
Ozturk et al. [8]	Classification in between COVID+, COVID−, and pneumonia X-ray	DarkCovidNet	COVID-19(+): 125 Pneumonia: 500 No-Findings: 500	2 class: 98.08% 3 class:87.02%
Apostolopoulos, Ioannis D., and Tzani A. Mpesiana [13]	Classification in between COVID, pneumonia, and normal X-ray	Convolutional neural network (CNN)	Dataset 1: COVID-19(+):224 Pneumonia: 700 No-Findings: 504 Dataset 2: COVID-19(+):224 Pneumonia: 714 No-Findings: 504	2 class: 96.78% 3 class: 94.72%
Narin, Ali, Ceren Kaya, and Ziynet Pamuk. [14]	Classification in between COVID-19 (+), and COVID-19 (−)	Deep CNN ResNet-50	COVID-19(+): 50 COVID-19 (−): 50	98%
Sethy, Prabira Kumar, and Santi Kumari Behera [15]	Classification in between COVID-19 (+), and COVID-19 (−)	ResNet50 + SVM	COVID-19(+): 25 COVID-19 (−): 25	95.38%
Abbas, Asmaa, Mohammed M. Abdelsamea, and Mohamed Medhat Gaber [16]	Classification in between COVID-19 (+), and COVID-19 (−)	DeTraC (Decompose, Transfer, and Compose) CNN model	COVID-19(+):105 SARS: 11 Normal: 80	95.12%
Zhang, Jianpeng, et al. [17]	Classification in between COVID-19 (+), and others	ResNet	COVID-19(+): 70 Others: 1008	Sensitivity: 0.96, Specificity: 0.71 AUC: 0.952
Wang, Linda, and Alexander Wong [18]	COVID and non-COVID X-ray classification	COVID-Net	COVID-19(+): 53 COVID-19 (−): 5526 Healthy: 8066	92.6%
Hemdan, Ezz El-Din, Marwa A. Shouman, and Mohamed Esmail Karar [19]	Classification in between COVID-19 (+), and normal X-ray	COVIDX-Net	COVID-19(+):25 Normal: 25	90%

2 Literature Review and Contribution of the Study

Accurate analysis of COVID-19 related X-ray images of the chest may serve as an initial detection scheme of abnormality in the medical domain. Existing studies detailed some methodologies for computerized automated COVID-19 detection using X-ray images. Ozturk et al. [8] developed a COVID-19 detection methodology using raw X-ray images of the chest. They performed classification in between COVID and no-findings and achieved 98.08% accuracy. In multiclass classification, they categorized COVID, no findings, and pneumonia and produced 87.02% accuracy. The DarkNet model used in their study for classification. Apostolopoulos, Ioannis D., and Tzani A. Mpesiana [13] applied the existing convolutional neural network (CNN) oriented transfer learning methodology for COVID, pneumonia, and normal X-ray classification. For 2 class classification, they got 96.78% accuracy using Deep-learning, and for three-class, maximum achieved accuracy is accuracy 94.72%. Narin, Ali, Ceren Kaya, and Ziynet Pamuk. [14] used deep transfer learning for the detection of COVID using X-ray images. Their study shows 98% classification accuracy using pre-trained ResNet50 architecture. The study performed by Sethy, Prabira Kumar, and Santi Kumari Behera [15] detected COVID affected X-ray images by combining the ResNet50 CNN model and support vector machine (SVM) classifier. The feature outcome of CNN is fed to SVM classifier for the categorization and obtained 95.38% accuracy. Abbas, Asmaa, Mohammed M. Abdelsamea, and Mohamed Medhat Gaber [16] performed a similar classification using deep CNN named as DeTraC (Decompose, Transfer, and Compose) model. Their obtained accuracy was 95.12% for classification. Zhang, Jianpeng, et al. [17] also did the same classification using deep learning methodology and obtained an accuracy of 96% for COVID-19 cases and 70.65% for non-COVID-19 cases. Wang, Linda, and Alexander Wong [18] achieved a classification accuracy of 92.6% for COVID and non-COVID X-ray categorization using COVID-Net deep CNN architecture. For classification in between COVID positive and COVID negative, Hemdan, Ezz El-Din, Marwa A. Shouman, and Mohamed Esmail Karar [19] used a deep learning network named as Covidx-net. Their maximum obtained accuracy is 90%.

Observation of the above review work indicates that existing work on X-ray image based COVID detection is performed by using deep learning-based CNN architecture. The maximum achieved accuracy is 98.08%. But, the existing works contain complex data models. Also, the use of deep learning requires high topological knowledge, deep parametric knowledge, and large dataset. Therefore it is difficult to adopt CNN architecture for the zone with less skilled manpower. Focusing on the scenario, in our study we focused on developing a simplified computerized methodology by using feature-based conventional classification strategy with optimal accuracy for X-ray image categorization aiming at COVID-19 detection.

Fig. 1 Flow diagram for X-ray image based COVID-19 detection

3 Methodologies of COVID-19 Detection

The chest X-ray image consists of salient features related to COVID-19. Computerized extraction of those features will help in the detection of the disease. In this study, we aim to develop a simplified methodology for chest X-ray image based abnormality detection. The methodology consists of only four important steps including data collection as shown in Fig. 1 and described below.

3.1 Data Collection and System Requirement

The analysis has been performed over two chest X-ray image datasets. The image data are collected from Kaggle repository (link: https://www.kaggle.com/tawsifurrahman/covid19-radiography-database) and database developed by Cohen JP (link: https://github.com/ieee8023/COVID-chestxraydataset). The dataset 1 contains both the COVID positive and negative X-ray images. In our study, we used all the 219 COVID positive X-ray images and 250 normal X-ray images. All the images are in Portable Network Graphics (PNG) file format. The size of each X-ray is 1024 × 1024 pixels. Most of the images are in a grayscale format where some are in color format. The color (RGB) images are converted into grayscale before processing. The dataset 2 also contains 125 COVID positive X-ray images, 500 pneumonia-related X-ray images, and 500 normal chest X-ray images. The images are of variable size and stored in png/jpg/jpeg format. We used the COVID-19 and normal X-ray images for this study. For both the dataset, COVID-19 oriented X-ray images are labeled as 1, and normal X-ray images are labeled as 0. The datasets are dedicated to research purposes and for the development of useful and impactful methodologies for COVID detection.

The overall is performed on MATLAB R2013a software. The system specification is Windows 10 with 64-bit Operating system, 4 GB RAM.

3.2 Feature Extraction

In this study, classification in between COVID-19 and normal raw chest X-ray images is performed by analyzing texture level features. The extracted features are

used as the input of the classifier as shown in Fig. 1. The details of the extracted features are given below.

a. **First-order statistical features** [20]:

Image pixel value-oriented simple statistical summary is extracted through first-order statistical features. The texture information related to the neighborhood intensity distribution of each pixel is not considered here. The histogram shows the rate of occurrence of each pixel intensity in an image. Based on each pixel intensity occurrence rate in the image the extracted first-order statistical features are mean, variance, kurtosis, skewness, standard deviation, entropy, and energy. A total of seven features are extracted from histogram characteristics.

b. **Spatial gray level dependence Matrices features** [21]:

Spatial gray level dependence Matrices features are calculated by extracting pixel intensity from 0°, 45°, 90°, and 135° angle with distance value 1 from center pixel (C). The horizontal pixels with center pixels are at 0° and the vertical pixels with C are at 90°. The top left and bottom right pixels for the 3 × 3 image are at 135° with the center. Finally, the bottom left and top right pixels from C are at 45° with the center. The Fig. 2 shows each pixel degree position clearly. 13 different features are extracted from special gray level dependence Matrices namely angular second moment, variance, contrast, correlation, local homogeneity, entropy, sum variance, difference variance, sum average, sum entropy, difference entropy, and information measure of correlation from x and y-axis (individually). All the mentioned features are extracted into two groups, mean group and difference group. In mean group average of feature value for a particular feature extracted from all the four angles are calculated. Similarly, in the difference group, the difference between the minimum and maximum values for a particular feature extracted from all four angles is calculated. Therefore a total of 26 features are extracted.

c. **Gray level difference statistics features** [22]:

The gray level difference based statistical features are calculated from X-ray images depending on the absolute difference present in between pairs of gray levels considering displacement ∂. For a given displacement ∂, four features are calculated. Those features are mean, contrast, entropy, and energy. The mentioned features are calculated considering $\partial = (0,1),(1,1),(1,0),(1,-1)$. Here $\partial \equiv (\Delta x, \Delta y)$.,

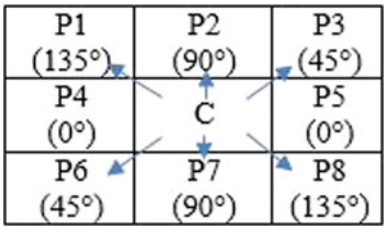

Fig. 2 Angular position of each pixel (P) from center pixel (C) for a 3 × 3 image

Therefore,∂ indicates a vector in (x, y) plane for an image $f(x, y)$. The mean value ∂ is taken for each feature.

d. **Neighborhood gray-tone difference matrix** [23]:

In image processing, information related to spatial changes in intensity distribution can be found by analyzing the gray tone of a pixel comparing with its neighborhood pixels. The neighborhood gray-tone difference matrix provides the same for spatial feature extraction. For the generation of the matrix, let $I(x, y)$ be the gray tone of a pixel at the position (x, y) having value i. Then the average gray tone considering 8-neighborhood pixels is,

$$P_i = P(x,y) = \frac{1}{W-1}\left[\sum_{m=-s}^{s}\sum_{n=-s}^{s} I(x+m, y+n)\right], (m,n) \neq (0,0)$$

Here, s represents the size of the neighborhood and $W = (2s+1)^2$.

Following the above, ith entry in the Neighborhood gray-tone difference matrix is,

$$N(i) = \begin{matrix} \sum \left| i - \overline{P_i}, \right| & \text{for } i \in A_i \text{ if } A_i \neq 0 \\ 0, & \text{otherwise} \end{matrix}$$

Here, $\{A_i\}$ is the set of all pixels with gray tone i.

Using the Neighborhood gray-tone difference matrix, five features are extracted in this study: Coarseness, contrast, complexity, busyness, and strength.

Coarseness indicates the uniformity in intensity distribution in an image. Higher the coarseness indicates increased uniformity in an image. In a coarse-textured image, the basic patterns related textures of the image are large. Therefore the intensity change is less in a coarse texture. The contrast of an image indicates the clarity in area based intensity change. High contrast indicates intensity difference in between neighborhood region is large. The feature Complexity of image depends on the presence of primitives or patches in a texture. A complex texture contains more patches that indicate content information is high in the image. The complexity of an image is also related to contrast and busyness features. The busyness of an image indicates a rapid change in intensity distribution compares to neighborhood intensity. Hence higher the frequency of spatial changes in pixel intensity values indicates greater busyness in an image.

The feature texture strength is complex to define. It is correlated with coarseness and contrast. In general, in a high texture strength-based image, the primitives that comprise it are clearly visible and definable. Such an image contains a high degree of visual clarity.

e. **Statistical feature matrix** [24]:

The statistical feature matrix performs a texture analysis of the image by measuring the statistical features of pixel pairs with multiple distances. In this statistical feature

matrix, the size of the matrix is based on the maximum distance considered, not on the gray level. The extracted properties in this study are coarseness, roughness, periodicity, and contrast. The study also considered the maximum inter-sample spacing distance as 4, i.e., $L_r = L_c = 4$.

f. **Texture energy measure** [25]:

LL, SS, EE, LE, LS, ES are six different kernels and generated from three simple vectors of length 3 for measuring texture energy. These are L3 ≡ (1, 2, l), S3 ≡ (−1, 2, −1), and E3 ≡ (−1, 0, 1). The vectors represent the one-dimensional operations of center-weighted local averaging, symmetric second differencing for spot detection, and symmetric first differencing for edge detection. If these vectors are convolved with themselves or with each other, we obtain five vectors of length 5. Those derived vectors are L5 = (1, 4, 6, 4, 1), S5 = (−1, 0, 2, 0, −1), E5 = (−1, −2, 0, 2, 1) where L5 again performs local averaging, S5 is spot detector, and E5 is the edge detector. Multiplying the column vectors of length 5 by row vectors of the same length, we obtain 5 × 5 masks. Using the masks, the texture energy is extracted by convolving them with the X-ray images. The final masks used in our experiments are as shown in Fig. 3. Finally, from this feature group, a total of six energy features are extracted from six different kernel/mask.

g. **Fourier power spectrum** [26]:

The Fourier transform of an image $I(x, y)$ is expressed as,

$$F(u,v) = \int_{-\infty}^{\infty} \int_{-\infty}^{\infty} e^{-2r\sqrt{-1(ux+vy)}} I(x,y)\mathrm{d}x\mathrm{d}y$$

The Fourier power spectrum is represented as $|F|^2 = FF^*$. Here * indicates the complex conjugate. In the case of a coarse-textured image, $|F|^2$ is high near the

LL:

1	4	6	4	1
4	16	24	16	4
6	24	36	24	6
4	16	24	16	4
1	4	6	4	1

SS:

1	0	-2	0	1
0	0	0	0	0
-2	0	4	0	-2
0	0	0	0	0
1	0	-2	0	1

EE:

1	2	0	-2	-1
2	4	0	-4	-2
0	0	0	0	0
-2	-4	0	4	2
-1	-2	0	2	1

LE:

-1	-2	0	2	1
-4	-8	0	8	4
-6	-12	0	12	6
-4	-8	0	8	4
-1	-2	0	2	1

LS:

-1	0	2	0	1
-4	0	8	0	4
-6	0	12	0	6
-4	0	8	0	4
-1	0	2	0	1

ES:

1	0	-2	0	-1
2	0	-4	0	-2
0	0	0	0	0
-2	0	4	0	2
-1	0	2	0	1

Fig. 3 Final kernels/masks for textural energy measure

origin. For fine texture, $|F|^2$ will be spread out more. To analyze the texture coarseness using the Fourier power spectrum, here in the study the annular-ring and wedge sampling features of X-ray images are extracted using the following equations.

Annular ring: $\phi_{x_1,x_2} \equiv \sum_{x_1^2 \le u^2+v^2<x_2^2} |F(u,v)|^2$

Wedge: $\phi_{\theta_1,\theta_2} = \sum_{\theta_1 < \tan^{-1}(v/u) < \theta_2} |F(u,v)|^2$

Here, x_1, x_2 our inner and outer ring radius. θ is wedge slope. In this study, the value of x_1, x_2 is 2, 4 and θ_1, θ_2 is $0°, 45°$ respectively. Also, $0 < u, v < P-1$ for a given $P \times P$ image.

3.3 Classification

The extracted features from chest X-ray images are fed to the classifier for COVID-19 abnormality detection. For that, four states of the art classifiers are used namely Support Vector Machine (SVM), Random Forest (RF), K Nearest Neighbour (KNN), and Linear Discriminant Analysis (LDA). The ten-fold cross-validation is performed for classifier accuracy analysis and 30% of the overall dataset is used for testing purposes. The parameter description of each classifier is mentioned here for a clear understanding.

SVM [27]: SVM classifier is a popularly used method for medical image classification. The required parameters for SVM are regularization parameter(C), kernel type, degree, and kernel coefficient. Here we used C = 1.0, linear kernel, and kernel coefficient as 0.1. The degree is not required here as we are using linear kernel for our analysis.

RF [20, 27]: RF classifier is designed based on combining multiple decision trees to obtain enhanced accuracy of classification. The required parameters for RF with values used for this study are number of tree: 100, quality of each split: Gini, the maximum number of feature for best split: auto, maximum tree depth: None, the minimum number of sample for the split: 20, the minimum size of end node/leaf:1, minimum weight fraction leaf: 0.0, maximum leaf node size: None, minimum impurity decrease: 0.0, bootstrap: True, cross-validation method (oob_score): False, processor number: None, random state: None, verbosity:0, warm_start: False, balanced subsample weight: None.

KNN [20, 27]: KNN is a simple, versatile, and easy to understand method of classification. The parameters tuning performed for KNN in this study are number of neighbors: 5, weight function: uniform, the algorithm used: auto, leaf size: 20, power parameter: 2, distance metric: Minkowski, arguments for metric function: None, number of parallel job for neighborhood search: None.

LDA [20, 27]: Through fitting class conditional density of the data and by using Bayes rule, the classifier generates a linear decision boundary for classification. In this study, the Singular value decomposition is used as a solver with rank estimation

threshold value 0.0001. The other parameters for the LDA classifier are set as the default value, i.e., None in this study.

3.4 Validation

The validation of the study outcome has been performed by comparing the result of the classification with clinical findings. Here seven validation parameters are used: true positive, true negative, false positive, false negative, sensitivity, specificity, and accuracy. True negative indicates that clinically COVID-19 marked X-ray images are accurately detected by the classifier. True positive is clinically normal detected X-ray images are also classified as normal through the classifier. False-negative indicates that clinically normal identified X-ray images are detected as COVID-19 through the classifier and false-positive is reverse of a false negative. The sensitivity, specificity, and accuracy are calculated by following the equations below.

$$\text{Sensitivity: } \frac{\text{True Positive}}{\text{True Positive} + \text{False Negative}}$$

$$\text{Specificity: } \frac{\text{True Negative}}{\text{True Negative} + \text{False Positive}}$$

$$\text{Accuracy: } \frac{\text{True Positive} + \text{True Negative}}{\text{True Positive} + \text{True Negative} + \text{False Positive} + \text{False Negative}} \times 100\%$$

Higher the value of all the measures indicates better performance of the classifier.

4 Results

In this study, the classification of the chest X-ray images for COVID-19 detection has been performed using the extracted textured features. A total of 55 features are extracted from seven different groups. The extracted features are fed to the four different classifiers with parameter tuning for optimal classification accuracy. The experiment has been performed over two datasets of COVID-19 X-ray images as mentioned in Sect. 3.1. Table 2 shows the outcome of classification using validation parameters. Observation of Table 2 shows that the Random Forest (RF) classifier generates maximum accuracy, i.e., 98.6% and 98.9% for both the dataset (dataset 1 and dataset 2) respectively. The sensitivity of the classifier is also maximum, i.e., 1 for both the datasets with specificity 0.97 and 0.95 respectively. Higher the sensitivity and specificity of classification indicates that most of the COVID-19 oriented X-ray images are accurately classified. The LDA classifier is also able to provide a high degree of classification with value 97.9% and 98.4% for datase1 and dataset 2 respectively. The classification outcome of each classifier is determined by taking the mean of ten-fold cross-validation. Figure 4 shows the

Table 2 Classification outcome

Classifier used	True positive	False negative	False positive	True negative	Sensitivity	Specificity	Accuracy (%)
Dataset 1							
SVM	71	2	15	53	0.97	0.78	87.9
RF	83	0	2	56	1	0.97	98.6
KNN	74	2	10	55	0.97	0.85	91.2
LDA	75	1	2	63	0.99	0.97	97.9
Dataset 2							
SVM	145	1	19	23	0.99	0.55	89.4
RF	145	0	2	41	1	0.95	98.9
KNN	144	3	14	27	0.98	0.66	90.9
LDA	146	1	2	39	0.99	0.95	98.4

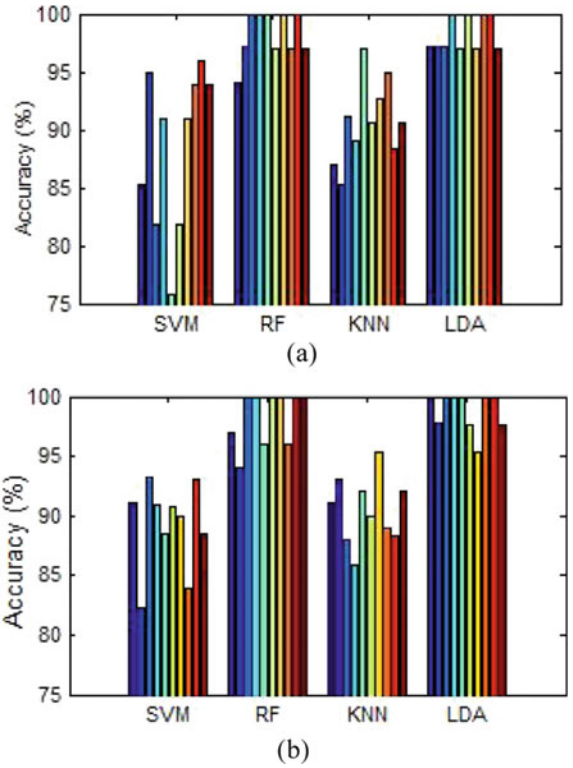

Fig. 4 Classification accuracy of each fold in ten-fold cross validation for **a** dataset 1, **b** dataset 2

accuracy of each fold for all the classifiers of both the datasets. Observation of Fig. 4 indicates that fold wise accuracies of SVM and KNN is highly variable and low compare to RF and LDA. For RF, fold base intra accuracies are very much similar to each other. As accuracy wise RF generates an optimal result of

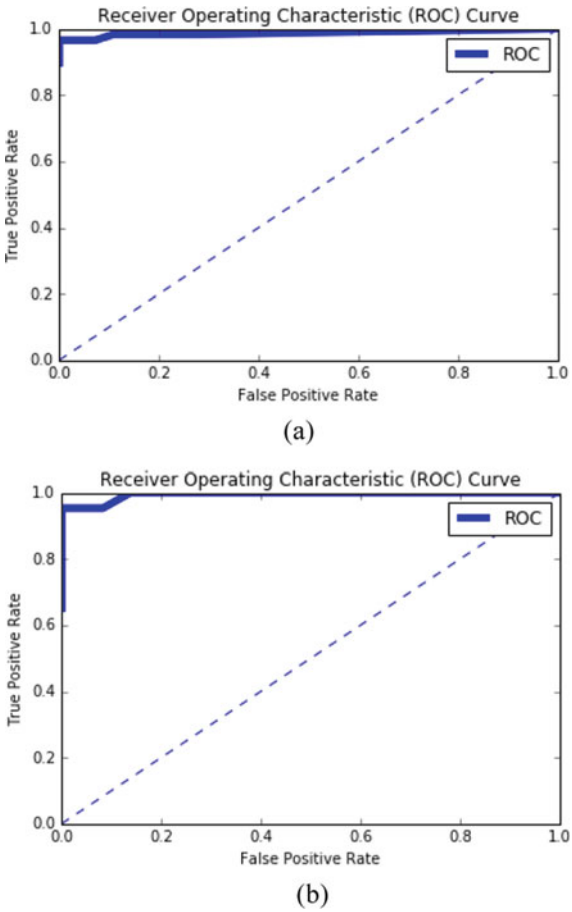

Fig. 5 ROC curve of RF classifier **a** dataset 1, **b** dataset 2

classification, so the Receiver Operating Characteristic (ROC) curve of RF outcome for both the dataset is given in Fig. 5. The area under the curve (AUC) for dataset 1 is 0.99 and dataset 2 is 1. The ROC curve also shows that RF classifier provides significant performance for X-ray image feature-based COVID-19 classification.

5 Discussion

The performance of the overall methodology is dependent on feature extraction and classifier selection. For optimal outcome, multiple classifiers are used as detailed in Sect. 3.3 and the effect of classifier in the accuracy of classification is shown in Table 2. In the case of feature extraction, a total of 55 texture features are extracted from seven different groups. Among them, some groups of features contain a higher

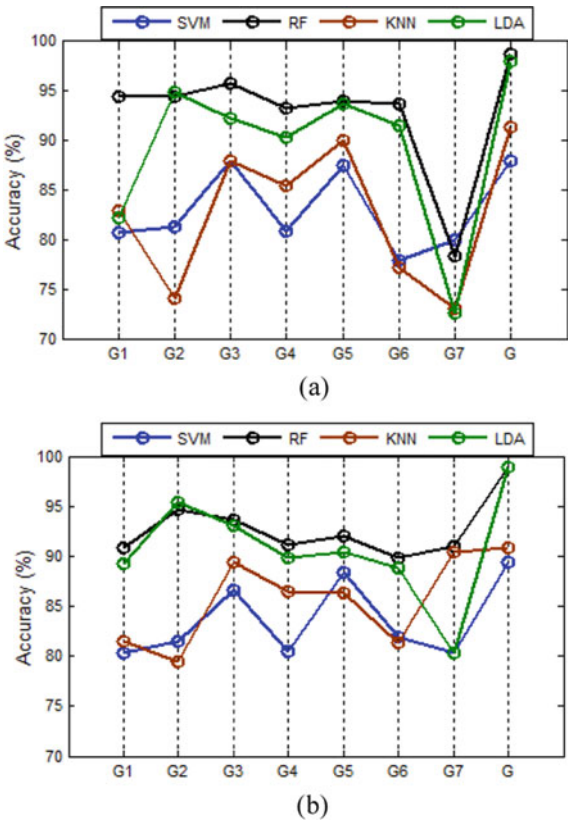

Fig. 6 Feature group base classication accuracy for **a** dataset 1, **b** dataset 2

degree of differentiable features for COVID oriented X-ray and normal X-ray classification. Figure 6 shows the classification accuracy of each group of features using four different classifiers. Here G1 to G7 represents seven different feature groups, i.e., G1: First order statistical features, G2: Spatial gray level dependence Matrices features, G3: Gray level difference statistics features, G4: Neighborhood gray-tone difference matrix features, G5: Statistical feature matrix features, G6: Texture energy measure features, G7: Fourier power spectrum features and G indicates the combination of all extracted features. The X-axis of Fig. 6 represents each group individually (G1 to G7) and G. Observation of Fig. 6 shows that in case of feature group- wise classification also, RF classifier generates optimal result for most of the groups. The G3 for dataset 1 and G2 for dataset 2 individually generates maximum accuracy of classification ($\leq 96\%$). But the combination of all feature groups (G) increases the accuracy of classification. The increase of accuracy through G is noticeable in the case of all four classifiers.

The maximum classification accuracy achieved through this study is 98.6% and 98.9% respectively for dataset 1 and dataset 2. Existing studies on X-ray image based COVID-19 classification also shows higher accuracy using CNN

Table 3 Comparative study of X-ray image based COVID-19(+) and COVID-19(−) classification

Study	Dataset details	Method used	Accuracy (%)
[8]	COVID-19(+): 125, No-Findings: 500	CNN (DarkCovidNet)	98.08
[13]	Dataset 1: COVID-19(+): 224, No-Findings: 504 Dataset 2: COVID-19(+): 224, No-Findings: 504	CNN	96.78
[14]	COVID-19(+): 50, COVID-19 (−): 50	CNN (Deep CNN, ResNet-50)	98
[15]	COVID-19(+): 25, COVID-19 (−): 25	CNN + SVM (ResNet50+)	95.38
[16]	COVID-19(+) and SARS: 116, Normal: 80	CNN(**DeTraC**))	95.12
[17]	COVID-19(+): 70, Others: 1008	CNN(ResNet)	Sensitivity: 0.96, Specificity: 0.71 AUC: 0.952
[18]	COVID-19(+): 53, COVID-19 (−) and healthy: 13,592	CNN (COVID-Net)	92.6
[19]	COVID-19(+): 25, Normal: 25	CNN (COVIDX-Net)	90
Our Study	Dataset 1: COVID-19(+): 219, Normal: 250 Dataset 2: COVID-19(+): 125, No-Findings: 500 (same dataset used in [8])	Texture Feature with Random Forest (RF) classifier.	Dataset 1: Sensitivity: 1, Specificity: 0.97, Accuracy: 98.6, AUC: 0.99 Dataset 2: Sensitivity: 1, Specificity: 0.95, Accuracy: 98.9, AUC: 1

architecture. Table 3 shows the comparative study of presented methodology and existing popular works on X-ray image base COVID detection. Observation shows that all the existing methodologies used the CNN architecture for classification and achieved a maximum 98.08% accuracy. In our study, we used the conventional classification strategy by extracting texture features of X-ray images and using those features as the input of the Random Forest (RF) classifier. The proposed conventional strategy of classification provides the highest accuracy among all existing studies. The used dataset 2 is as same as the dataset used by Ozturk et al. [8] in their study.

6 Conclusion

COVID-19 is the infectious disease caused by the most recently discovered coronavirus. This new virus and disease were unknown before the outbreak began in Wuhan, China, in December 2019. COVID-19 is now a pandemic affecting many countries globally [28–32]. This study proposes a conventional feature extraction-based method for COVID-19 detection using chest X-ray image datasets. The method is applied over two datasets and generates 98.6% and 98.9% accuracy of classification in between COVID affected X-ray images and normal X-ray images using RF classifier with AUC as 0.99 and 1 respectively. A total of 55 texture features are extracted for this purpose from seven different groups. Group-wise analysis of classification shows that individually Gray level difference statistics features (G3) and Spatial gray level dependence Matrices features (G2) for dataset 1 and dataset 2 respectively generate maximum accuracy of 95.7% (using RF classifier) and 95.4% (using LDA classifier). A combination of all the feature groups improves the accuracy by 2.9% and 3.5% for dataset 1 and dataset 2 respectively. The existing popular studies of the same classification generates a maximum accuracy of 98.08% using CNN architecture. Also, the use of feature extraction dependent conventional classification methodology is not present in existing studies. Though CNN architectures are used for X-ray image base COVID classification but contain the difficulty related to a limited number of image data, the requirement of data augmentation, architecture complexity, hyper-parameter tuning, slow processing, and lack of expert knowledge. Our suggested method generates better accuracy compared to CNN based methods for COVID-19 classification and also less complex, faster, and applicable for small datasets. The future direction of the method will aim to identify the region of abnormality in the chest using CT and X-ray images.

Acknowledgements Authors would also like to thank Dr. M.K. Bhowmik, Assistant Professor, Department of Computer Science and Engineering, Tripura University, Suryamaninagar 799022, Tripura, India for his support during knowledge development in the area of image feature extraction and classification.

References

1. Singhal, T.: A review of coronavirus disease-2019 (COVID-19). Indian J. Pediatr. 1–6 (2020)
2. Coronavirus.: https://www.who.int/emergencies/diseases/novel-coronavirus-2019 (2020). Retrieved 27 May 2020
3. W. H. Organization.: Clinical management of severe acute respiratory infection when Novel coronavirus (2019-nCoV) infection is suspected: interim Guidance
4. National Health Commission of the People's Republic of China, Diagnosis and treatment protocol for COVID-19 (trial version 7). http://en.nhc.gov.cn/2020-03/29/c_78469.htm
5. Ai, T., et al.: Correlation of chest CT and RT-PCR testing in coronavirus disease 2019 (COVID-19) in China: a report of 1014 cases. Radiology. 200642 (2020)

6. Fu, H., et al.: Association between clinical, laboratory and CT characteristics and RT-PCR Results in the follow-up of COVID-19 patients. medRxiv (2020)
7. Dong, D., Tang, Z., Wang, S., et al.: The role of imaging in the detection and management of COVID-19: a review [published online ahead of print, 2020 Apr 27]. IEEE Rev. Biomed. Eng. (2020). https://doi.org/10.1109/rbme.2020.2990959. https://doi.org/10.1109/rbme.2020.2990959
8. Ozturk, T., et al.: Automated detection of COVID-19 cases using deep neural networks with X-ray images. Comput. Biol. Med. 103792 (2020)
9. Xie, X., Zhong, Z., Zhao, W., Zheng, C., Wang, F., Liu, J.: Chest CT for typical 2019-nCoV pneumonia: relationship to negative RT-PCR testing. Radiology (2020)
10. Shi, H., et al.: Radiological findings from 81 patients with COVID-19 pneumonia in Wuhan, China: a descriptive study. Lancet. Infect. Diseas. 242020 (2020). https://doi.org/10.1016/s1473-3099(20)30086-4
11. Kanne, J.P.: Chest CT findings in 2019 novel coronavirus (2019-nCoV) infections from Wuhan, China: key points for the radiologist. Radiology **295**(1), 16–17 (2020). https://doi.org/10.1148/radiol.2020200241
12. Jacobi, A., et al.: Portable chest X-ray in coronavirus disease-19 (COVID-19): a pictorial review. Clin. Imaging. **64**, 35–42 (2020). https://doi.org/10.1016/j.clinimag.2020.04.001apostolopoulos
13. Apostolopoulos, I.D., Mpesiana, T.A.: Covid-19: automatic detection from x-ray images utilizing transfer learning with convolutional neural networks. Phys. Eng. Sci. Med. 1 (2020)
14. Narin, A., Kaya, C., Pamuk, Z.: Automatic detection of coronavirus disease (COVID-19) using x-ray images and deep convolutional neural networks. Preprint at arXiv:2003.10849 (2020)
15. Sethy, P.K., Behera, S.K.: Detection of coronavirus disease (COVID-19) based on deep features. Preprints 2020030300 (2020)
16. Abbas, A., Abdelsamea, M.M., Gaber, M.M.: Classification of COVID-19 in chest X-ray images using DeTraC deep convolutional neural network. Preprint at arXiv:2003.13815 (2020)
17. Zhang, J., et al.: Covid-19 screening on chest x-ray images using deep learning based anomaly detection. Preprint at arXiv:2003.12338 (2020)
18. Wang, L., Wong, A.: COVID-Net: a tailored deep convolutional neural network design for detection of COVID-19 cases from chest X-Ray images. Preprint at arXiv:2003.09871 (2020)
19. Hemdan, E.E.D., Shouman, M.A., Karar, M.E.: Covidx-net: a framework of deep learning classifiers to diagnose covid-19 in x-ray images. Preprint at arXiv:2003.11055 (2020)
20. Bhowmik, M.K., et al (2017) Designing of ground truth annotated DBT-TU-JU breast thermogram database towards early abnormality prediction. IEEE J. Biomed. Health Inf. https://doi.org/10.1109/jbhi.2017.27405.00
21. Haralick, R.M., et al.: Textural features for image classification. IEEE Trans. Syst. Man. Cybern. SMC. **3**(6), 610–621 (1973). https://doi.org/10.1109/tsmc.1973.43093.14
22. Weszka, J.S., et al.: A comparative study of texture measures for terrain classification. IEEE Trans. Syst. Man. Cybern. SMC. **64**, 269–285 (1976). https://doi.org/10.1109/tsmc.1976.54087.77
23. Amadasun, M., King, R.: Textural features corresponding to textural properties. IEEE Trans. Syst. Man. Cybern. **19**(5), 1264–1274 (1989). https://doi.org/10.1109/21.44046
24. Wu, C.M., Chen, Y.C.: Statistical feature matrix for texture analysis. CVGIP Graph Models Image Process. **54**(5), 407–419 (1992). https://doi.org/10.1016/1049-9652(92)90025-s
25. Laws, K.I.: Texture energy measures. DARPA Image Understanding Workshop, pp. 47–51. DARPA, Los Altos, CA (1979)
26. Wu, C.M., et al.: Texture features for classification of ultrasonic liver images. IEEE Trans. Med. Imaging. **11**(2), 141–152 (1992). https://doi.org/10.1109/42.141636
27. Guyon, I., Weston, J., Barnhill, S., Bapnik, V.: Gene selection for cancer classification using support vector machines. Mach. Learn. **46**(1–3), 389–422 (2002)

28. Arpaci, I., Alshehabi, S., Al-Emran, M., Khasawneh, M., Mahariq, I., Abdeljawad, T., Hassanien, A.E.: Analysis of Twitter data using evolutionary clustering during the COVID-19 pandemic. Comput. Mater. Continua. **65**(1), 193–204 (2020). https://doi.org/10.32604/cmc.2020.011489
29. Arpaci, I., Karataş, K., Baloğlu, M.: The development and initial tests for the psychometric properties of the COVID-19 Phobia Scale (C19P-S). Personality Individ. Differ. **164**, 110108 (2020). https://doi.org/10.1016/j.paid.2020.110108
30. Arpaci, I.: A hybrid modeling approach for predicting the educational use of mobile cloud computing services in higher education. Comput. Hum. Behav. **90**, 181–187 (2019). https://doi.org/10.1016/j.chb.2018.09.005
31. Arpaci, I., Al-Emran, M., Al-Sharafi, M.A., Shaalan, K.: A novel approach for predicting the adoption of smartwatches using machine learning algorithms. In: Recent Advances in Intelligent Systems and Smart Applications, pp. 185–195. Springer, Cham (2021)
32. Arpaci, I.: What drives students' online self-disclosure behavior on social media? A hybrid SEM and artificial intelligence approach. Int. J. Mobile Commun. **18**(1) (2020). https://doi.org/10.1504/IJMC.2020.105847